

GEOMETRIC VARIABILITY AND ITS INFLUENCE ON STEADY AND UNSTEADY FAN AERODYNAMIC PERFORMANCE

R. Schnell, G. Ashcroft

German Aerospace Center DLR, Linder Hoehe, 51147 Cologne

Keywords: *CRTF, Fan design and testing, Geometric Variability, Uncertainty, Harmonic Balance, Blade Row Interaction*

Abstract *The paper deals with the appraisal and quantification of the uncertainty in predicting the aerodynamic performance of a contra-rotating turbo fan, here mainly due to geometric variations stemming from the manufacturing process. The investigated fan, comprising of two consecutive, contra-rotating rotors, was designed in the context of the European project VITAL. To assess the manufacturing quality and resulting effects of geometric variability on fan aerodynamic performance, the geometry of the entire first rotor was measured using a highly accurate optical scanning device. The paper comprises of three parts: In the first part the uncertainty in predicting overall fan performance based on 3D steady state RANS computations will be discussed. Here the focus will be on a discussion of the scattering of the main performance indicators as well as the radial distributions of the most important circumferentially averaged flow quantities. The second part deals with the analysis of results from full annulus computations of the real (scanned) rotor geometry in comparison with the idealized single passage simulation of the nominal geometry. As it will be seen in the pressure spectra the full annulus computations exhibit an enriched spectrum with harmonics not only present at multiples of the rotors blade number as for the single-passage solution, but almost all engine order harmonics can be found well above numerical noise levels. The last part focusses on the assessment of real geometry effects on unsteady wake-blade interaction. The focus here will be to investigate the change in wake structure downstream of the first rotor induced by real geometry effects and how this changes the response of the aft rotor in terms of*

its blade pressure amplitudes. In order to efficiently simulate the blade row interaction, a newly developed Harmonic-Balance method will be introduced and applied, allowing for a detailed study of the non-linear blade row interaction based on harmonic decomposition of the flow field.

1 Introduction

As part of its dedicated research activities related to potential fan concepts for future ultra-high bypass ratio aero engines, the German Aerospace Center (DLR) designed and coordinated the manufacturing of a contra-rotating turbofan in the context of the European project VITAL. The overall effort was led by Snecma, who provided the global specifications and the overall test logic, the coupled aerodynamic and mechanical design of this version CRTF2b was carried out at the Institute of Propulsion Technology of DLR in Cologne, final and detailed mechanical assessment was carried out at DLR's Institute of Structures and Design. The test rig was built and tested at CIAM compressor test facilities in Moscow (see Figure 1), the measured performance characteristics of the stage in comparison with post-test CFD results along with a more detailed summary of the major specifications and available test results were already reported in [7].

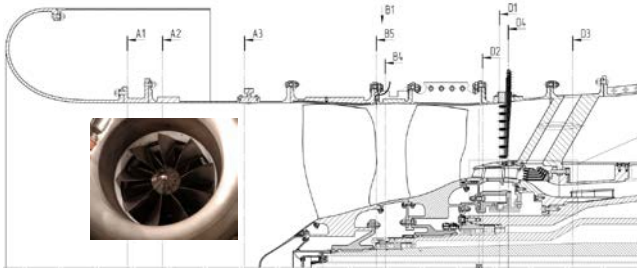


Figure 1: Sketch of the contra rotating turbo fan rig CRTF2b installed at CIAM compressor test bed C-3A

The rig comprised of two contra rotating rotors (Figure 2) which were manufactured as titanium blisks by CNC controlled five-axis milling machines. To assess the manufacturing quality, the entire first rotor was geometrically measured using a highly accurate optical scanning device, the results of this scanning process are summarized in [10], also including an assessment of the effect of the instrumentation on aerodynamic performance as well as boundary layer transitional behavior.



Figure 2: Rotor 1 blisk with strain gauge instrumentation (left) and CRTF2b fan stage assembly (right)

2 Aerodynamic Performance

The numerical setup used for this study was identical to the one described in [7] where the block structured grid comprised of approximately 6.3 million cells with y^+ values around unity on all blade surfaces. The computational domain covered a part of the inlet to the first rotor including the spinner, the second rotor including a large part of the bypass channel, a small portion of the duct to the booster stage and the bypass/core flow separator located downstream of the first rotor (see Figure 1). All fully turbulent RANS simulations were

carried out with DLRs turbomachinery CFD solver TRACE [1] involving a modified Wilcox $k-\omega$ turbulence model and with mixing planes in between both blade rows. The (undeformed) geometry of each scanned rotor 1 blade was processed and meshed in an identical way, whereas the rest of the stage was kept as it was, resulting in nine full stage single-passage CFD simulations for each operating point on the selected 100% speed line. For all nine setups the static pressure at bypass and core outlet was kept constant for each operating point. The convergence criteria were set rather tight for all operating points in order for the results to solely reflect the differences of the geometry; here the convergence related and remaining variations of the aerodynamic performance data (mass flow rate, pressure ratio and efficiency) including the resulting mass flow error were in the order of 10^{-3} % and thus for the majority of the results more than one order of magnitude smaller than the observed variations due to the different blade geometries. Based on the individual single passage CFD simulations for each blade, the scattering of the main performance parameters such as mass flow rate, rotor 1 total pressure ratio and efficiency was assessed for each operating point on the 100% speedline (Figure 3 and Figure 4). Only a portion of the entire speedline was calculated, with the last point (7) yielding a point close to the numerical stability limit and the first point just before rotor 2 choking (1). The definition of the operating points (1)-(7) is provided in Figure 3 and Figure 4 also, along with the individual results for all nine scanned blades. Furthermore, the global statistical properties for each quantity in terms of the average and the standard deviation were derived; the results are also shown in the given figures. Despite the relatively low number of samples it is assumed that the prediction accuracy of the expectancy value and standard deviation yield the proper trends (in fact the standard error for a population of n samples is in the order of $\sigma/n^{1/2}$) and thus provide a rather good estimate for the amount of scattering of the aerodynamic performance data induced by the given geometric variability.

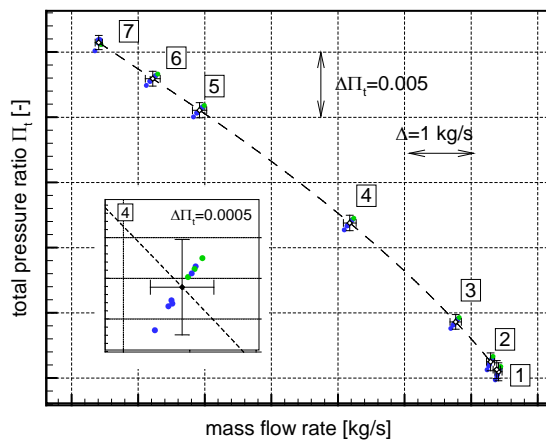


Figure 3: Rotor 1 total pressure ratio at 100% rotational speed based on 3D-CFD full stage simulations for all nine scanned rotor 1 blades and derived standard deviation ($\pm 2\sigma$)

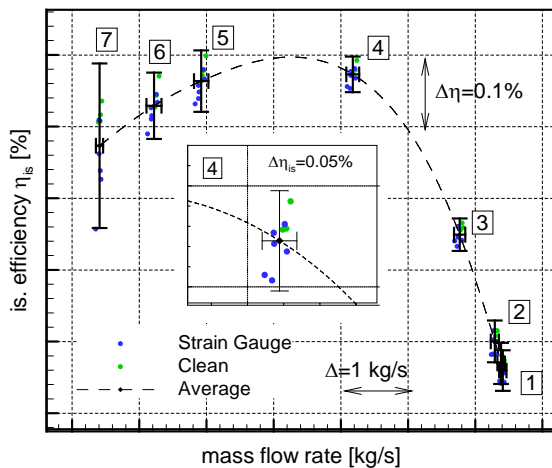


Figure 4: Rotor 1 isentropic efficiency at 100% rotational speed based on 3D-CFD full stage simulations for all nine scanned rotor 1 blades and derived standard deviation ($\pm 2\sigma$)

In terms of isentropic efficiency, most of the observed variations are within an interval of $\Delta\eta=\pm 0.05\%$, with a slight increase of efficiency variances towards higher rotor loading. The last stable point yielded significantly higher values of $\Delta\eta_{is}=\pm 0.1$, although it should be taken into account that the convergence of this point was not as good as for the other points. The maximum mass flow rate variations (min/max) are in the order of 0.1-0.2 kg/s, which is approximately 0.2-0.4% of the total mass flow rate. The total pressure ratio variation as shown in Figure 3 is very small and almost constant over the entire speedline. Bearing in mind the

comparison between measured and simulated stage as discussed in [6] and [10], one can already conclude that the geometric blade to blade variations and their effect on aero performance is small compared with the discrepancies between measurement and simulations. Figure 5 finally shows the radial distributions of the total pressure and relative flow angle at different positions along the stage and for all nine blades in a direct comparison. Exemplarily for a radius close to the blade tip at approximately 90% span the rectangles within the diagrams show the resulting scattering which are in accordance with the shown performance results. The min-to-max variations of the total pressure are in the order of 150 Pa, whereas the resulting changes in the relative outflow angle are approximately 0.1° . Also, as it will be discussed later, the propagation of the variances through the second rotor does not induce to a significant change thereof.

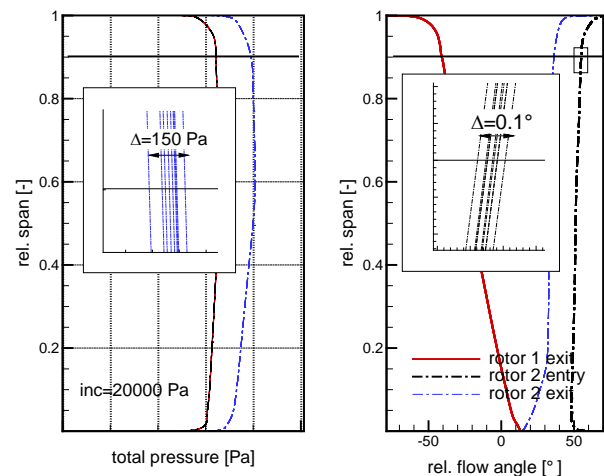


Figure 5: Radial distributions of circumferentially averaged total pressure (left) and relative outflow angle (right) – results for all nine scanned blades are shown at rotor 1 exit, rotor 2 entry and rotor 2 exit for operating point [4]

Finally the question shall be addressed how the rotor 1 geometrically induced efficiency uncertainties impact on the overall stage efficiency. Therefore the resulting standard deviations of both, rotor 1 as well as corresponding stage efficiency values are shown in Figure 6 for three selected operating points. As can be seen, the resulting stage efficiency

variance is always lower than rotor 1 efficiency variance by 20% up to 50%, depending on the operating conditions. Whereas the rotor 1 efficiency variance is a direct result of its geometric variability, the resulting stage efficiency variation is being imposed by a variance of the rotor 2 inlet conditions being imposed by the first rotor and its varying outflow quantities. To understand why the stage efficiency uncertainty decreases compared with the rotor 1 efficiency, we consider a constant propagation of the variances through the second rotor, associated with a linear transmission characteristic of the rotor 1 outflow quantities. The equation for the isentropic efficiency

$$\eta_{is} = \frac{\pi_t^{\frac{\gamma-1}{\gamma}} - 1}{T_{t2}/T_{t1} - 1} \quad (1)$$

can be used to express the change in isentropic efficiency $\Delta\eta_{is}$ as a function of the total pressure variation $\Delta\pi_t$ at different total pressure levels as shown in Figure 7. As it can be seen, the dependency is almost linear for the given range between $\Delta\pi_t = \pm 0.00075$, which was directly derived from the results shown in Figure 3. Furthermore, the slope of this linear relation increases with lower pressure ratios so that at low pressure ratios $\pi_{t,3}$ the resulting change in isentropic efficiency $\Delta\eta_{is}$ is almost twice the value of the corresponding change at higher pressure ratio $\pi_{t,1}$ for a given total pressure variation of $\Delta\pi_t = 0.0005$. Since the total pressure level at rotor 2 exit is significantly higher than at rotor 1 exit, the resulting change in stage efficiency for a given total pressure variance is almost lower than the rotor efficiency. Similar considerations can be made taking into account the resulting changes of the total temperature (which here was found to be less influential).

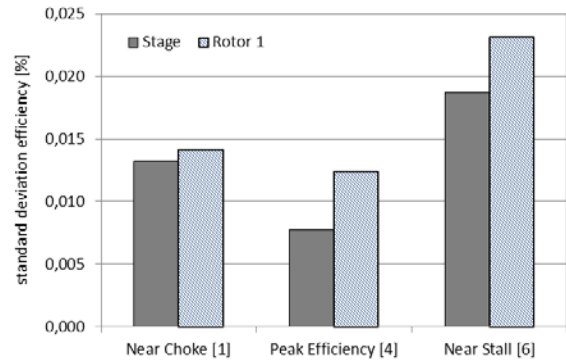


Figure 6: Comparison between stage and rotor isentropic efficiency standard deviation at 3 selected operating conditions

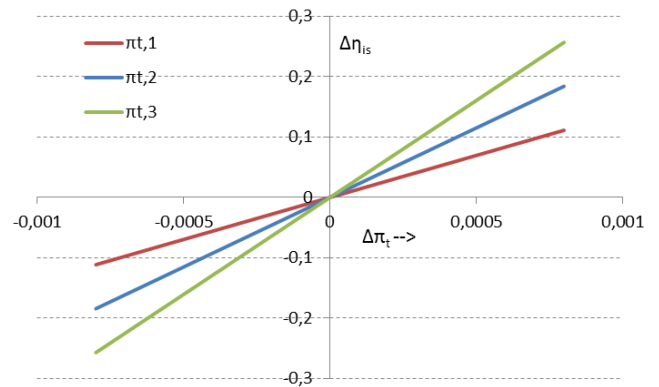


Figure 7: Change in isentropic efficiency $\Delta\eta_{is}$ as a function of total pressure variations $\Delta\pi_t$ at different total pressure levels with $\pi_{t,1} < \pi_{t,2} < \pi_{t,3}$

3 Results from Rotor 1 Steady State Full Annulus Computations

In addition to the shown performance parameters based on individual RANS computations of the separate blades, results from steady-state computations of the entire blisk comprising of all nine blades of the real (scanned) rotor 1 geometry in comparison with the idealized single passage simulation of the nominal geometry shall be discussed now. The focus will be on rotor-1 shock system as shown in Figure 8 and its blade-to-blade variation. The shown pressure contours yield a rather wavy structure since results from the 3D grid were interpolated onto a surface at constant radius and with equidistant circumferential resolution in order to perform the harmonic analysis. Whereas the resolution in azimuthal direction was kept from the CFD grid, it was reduced in

axial direction, which led to the visible structure of the pressure contours. As can be seen in the pressure spectra shown in Figure 9, the full annulus computations exhibit an enriched spectrum with harmonics not only present at multiples of the rotors blade number as for the single-passage solution, but almost all engine order harmonics can be found well above numerical noise levels. Although the shown spectrum of the real geometry does not exactly yield multiple-tone harmonics typical for buzz-saw noise, the scattering of the harmonics is caused by blade-to-blade shock system variations due to the geometrical differences in the rotor leading edge geometry.

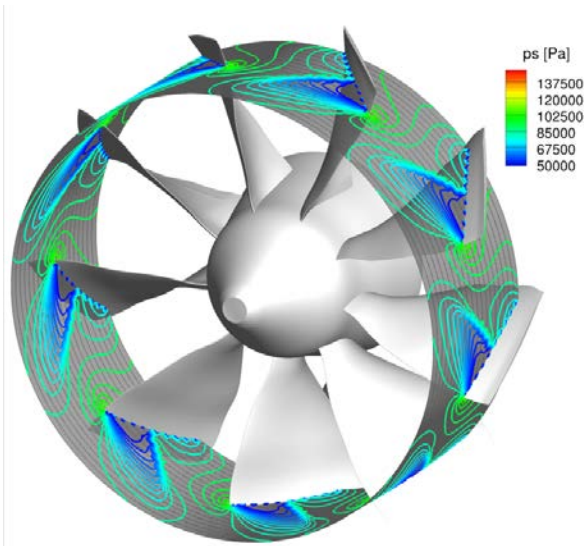


Figure 8: Shock system at approximately 90% span based on steady state full annulus computations of the real (scanned) blade geometry

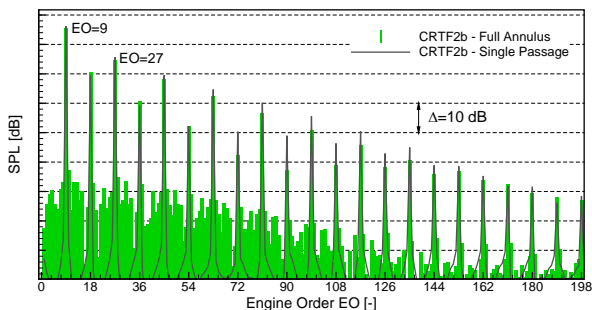


Figure 9: Pressure spectra (spatial) upstream of the first rotor; comparison of the idealized single passage solution (black lines) with results based on full annulus computations (green lines)

4 Unsteady Blade Row Interaction

4.1 Harmonic Balance Method Description

In order to assess the resulting uncertainty in the prediction of unsteady blade row interaction, fully coupled single-passage simulations of the entire CRTF stage comprising of both rotors were carried out. In order to efficiently carry out these often very time consuming simulations, a newly developed method based on a harmonic-balance (HB) approach, capable of simulating all kinds of time-periodic, nonlinear phenomena was applied. The method employed here is an alternating frequency-time domain technique. It is based on the direct use of the nonlinear residual functions and their discrete Fourier transforms, with similar approaches originally being introduced in [5] and [6]. The implementation of this particular method, its verification and application to turbomachinery relevant unsteady flows, also focusing on blade row coupling and boundary conditions, is described in detail in [1]. The application of this HB approach enabled a drastic reduction of the overall computational effort compared with fully non-linear computations, whilst fully capturing all linear and nonlinear effects for any (pre-defined) frequency or harmonic of the interaction frequency respectively. For this particular study five harmonics as well as the time average were taken into account and the resulting interaction was computed for each individual rotor 1 blade in combination with the nominal rotor 2 blade taking advantage of the individual single passage setups discussed in the previous section of this paper. Only results for the peak efficiency point at nominal rotational speed will be considered.

4.1 Results

The results in Figure 10 are shown to visualize the major blade row interaction phenomena, here exemplarily for a transonic section at 70% radius and based on the instantaneous flow field: The most dominant phenomenon is the upstream interaction of the aft rotor shock (Figure 10, left), which periodically impinges on the aft part of the front

rotor and induces very high amplitudes of the resulting pressure fluctuations, here reaching values up to 10%-15% of the ambient static pressure for the first BPF harmonic. Apart from the upstream interaction, the rotor 1 wakes impinge on the aft rotor blade and the induced flow incidence periodically changes the stagnation point and hence induces a varying pressure on the blade surface (Figure 10, right). However, this effect, compared with the upstream interaction is less dominant and the resulting blade pressure amplitudes are significantly lower [10].

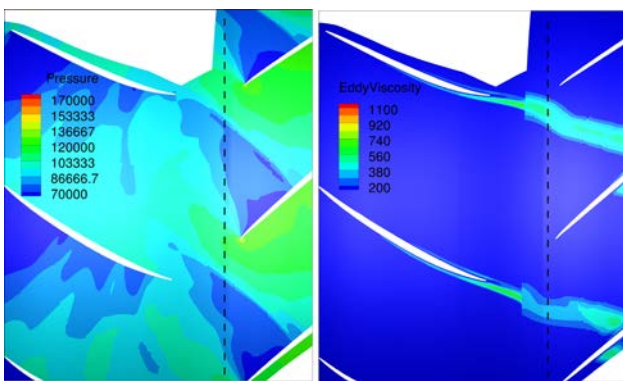


Figure 10: Instantaneous flow field at approximately 70% span highlighting the major interaction phenomena: upstream shock/blade interaction visualized by static pressure contours (left) and downstream wake/blade interaction visualized by contours of eddy viscosity (right) - results from HB computations with 5 harmonics

Before focusing on the blade pressure fluctuations and their corresponding variances themselves, the variations in rotor 1 wake depth as the main driver of the aft rotor pressure amplitudes shall be discussed. Therefore the spatial evolution of the instantaneous axial velocity just upstream of the aft rotor for all nine blades is shown in Figure 11, in which the corresponding velocity deficits of the front rotor wakes and their variations from blade to blade can be seen. The observed circumferential variation of the velocity however, not only contains portions of the front rotor wake, but also the acceleration and shock related diffusion areas of the aft rotor. The lower plot in Figure 11 (b) focusses on the front rotor wake region and it can be seen that the blade to blade

variations of the wake deficit are in the order of 5 m/s, which directly translate to variations in the aft rotor blade pressure amplitude. Also the variances in the shock region, here also expressed as fluctuations of the axial velocity, are in a similar order and mainly induce variations of the front rotor pressure amplitudes due to the upstream interaction. These pressure amplitudes are shown in Figure 12 at different fractions of the span for all nine blades. It can be seen that the maximum scattering between the nine blades occurs in the aft region of the front rotor just downstream of the shock and the resulting variations in the peak amplitude are in the order of up to 1500-1700 Pa at 90% span, whereas the shock itself always appears to be at the very same position. The wake-induced variations on the rotor 2 surface are of much lower amplitude, almost constant along the pressure side and very small in the expansion region upstream of the shock. Close to the hub and at mid span, where the flow regime is entirely subsonic, the absolute value of the variations are much lower, in the order of 200-500 Pa and more or less constantly distributed among both blade rows.

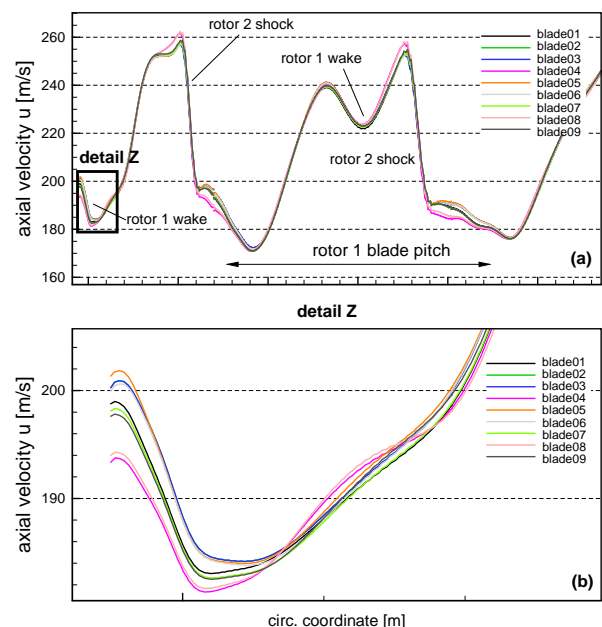


Figure 11: Instantaneous axial velocity just upstream of the leading edge of the second rotor for all nine blades (the axial position is denoted in Figure 10)

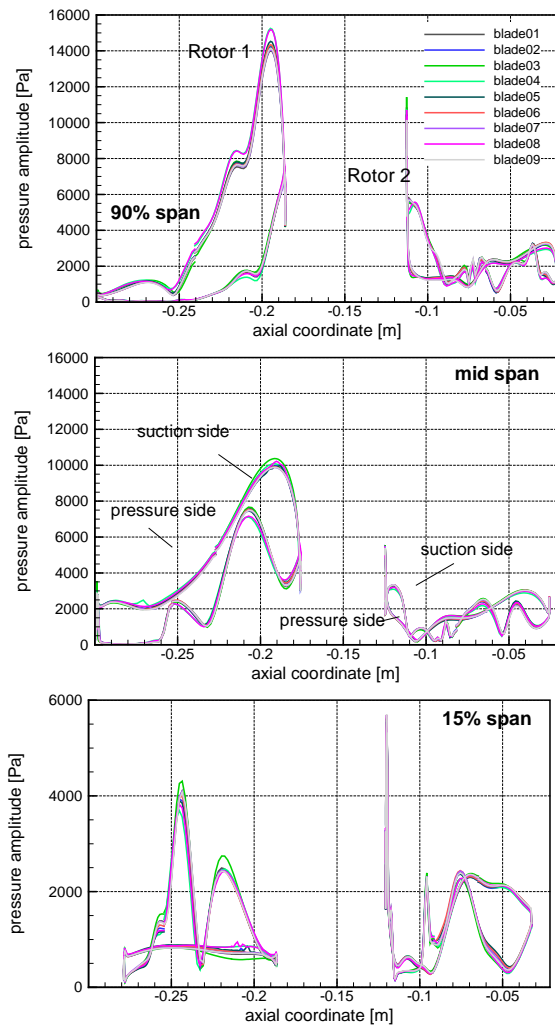


Figure 12: Blade surface static pressure amplitudes (1st relative BPF harmonic) resulting from unsteady blade row interaction at different radial positions

In order to assess the entire uncertainty of the calculated blade surface pressure amplitude, which is important for both, forced response estimations as well as for the resulting tonal noise emission, the local standard deviation of the pressure amplitude was calculated based on the unsteady computations of each individual blade. It is expected that two major effects can be seen in the results: the first one being the change in blade geometry and hence a local change of the shock system and blade wake which simply changes the locus of the interaction pattern. The second effect, which is considered to be of lower significance, is the change in operating conditions as already discussed by means of the stage performance characteristics. The resulting uncertainty in

predicting the blade surface pressure amplitude is shown in Figure 13 and Figure 14 in terms of its standard deviation of the first 2 (relative) BPF harmonics. It can be seen that the maximum resulting uncertainty is located in the aft part of the front rotor with values as high as up to 1300 Pa on the front rotor (Figure 13, top left) and 2000 Pa on the pressure side (Figure 14) for the first harmonic. The region of this high uncertainty is spatially limited to the area downstream of the rotor 1 shock, suggesting that the rotor 1 shock position itself is hardly affected by the geometric variations and the major impact is the upstream interaction of the aft rotor shock system. The location of the highest uncertainty is the same for the second harmonic, but standard deviations drop down to about half of the values given for the first harmonic. The shock on the aft rotor suction also is very pronounced in terms of an increased standard deviation, which is mainly caused by the variations in the front rotor wakes and a resulting shock position variation. A second observation is that the uncertainty in wake-induced pressure variations in the aft rotor is, as the interaction itself, much lower and hardly above 300-500 Pa for the first BPF harmonic and even lower for the second harmonic.

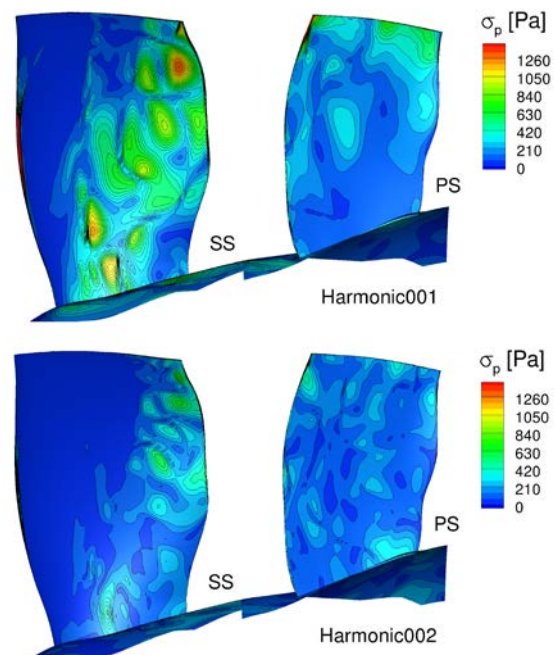


Figure 13: Resulting uncertainty of the blade pressure amplitude in terms of the standard deviation as directly derived from HB

simulations for all nine blades - shown are results of the 1st and 2nd harmonic at rotor 1 SS (left) and rotor 2 PS (right)

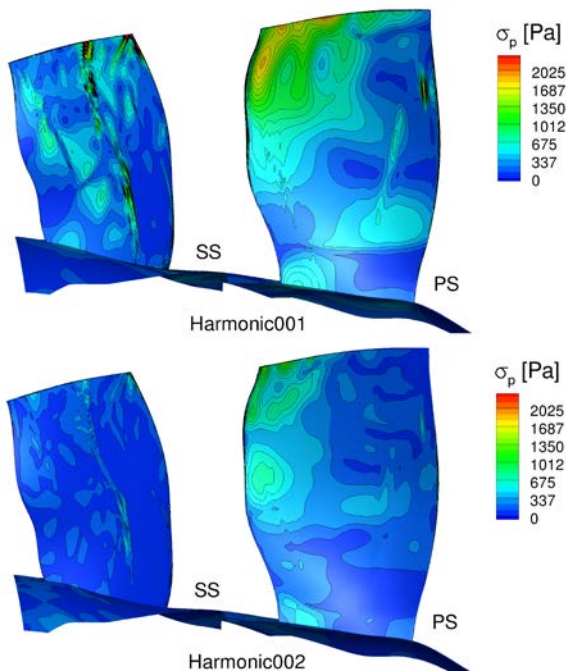


Figure 14: Resulting uncertainty of the blade pressure amplitude in terms of the standard deviation as directly derived from HB simulations for all nine blades - shown are results of the 1st and 2nd harmonic at rotor 1 PS (right) and rotor 2 SS (left)

Summary and Conclusions

The present paper dealt with an assessment of the influence of geometric variability on the aerodynamic performance of a contra rotating turbofan. In the first part the uncertainty in predicting the overall fan performance based on 3D steady state RANS computations was discussed and quantified. Here the effect on integral performance parameters was found to be in the order of 0.1-0.2% for the mass flow rate. The standard deviation of the efficiency was increasing towards higher rotor blade loading and reached values up to +/-0.1% for an operating point close to stall. The standard deviation of the total pressure ratio was almost constant over the entire speed line and in the order of +/-0.0005. Corresponding error

propagation was also considered and it was found that the uncertainty in stage efficiency was always significantly lower than rotor efficiency. Apart from integral parameters, the radial distribution of several flow parameters and in particular their scattering was shown and quantified also. Based on RANS computations of the entire blisk it was shown that the shown pressure harmonics exhibited an enriched spectrum with harmonics not only present at multiples of the rotors blade number as for the single-passage solution, but almost all engine order harmonics were found well above numerical noise levels. Furthermore, the effect of geometric variability on unsteady blade row interaction was investigated applying a novel and efficient harmonic balance method. Here first of all the resulting scattering in the rotor 1 wake depth was analyzed and quantified. The scattering of the blade row interaction due to the geometric variability was also quantified based on blade pressure amplitudes of various harmonics. Here it was shown that the upstream rotor 2 shock with the aft part of the first rotor was dominant on an absolute basis. Also the resulting uncertainty was highest in this region, whereas the scattering in wake/blade interaction, assessed by means of the pressure amplitudes on the aft rotor blade surface, was less d.

References

- [1] Frey, C., Ashcroft, G., Kersken, H.-P., Voigt, C.: *A Harmonic Balance Technique for Turbomachinery Applications*, ASME Paper GT-2014-25230, ASME Turbo Expo Düsseldorf/Germany, 2014
- [2] Franke, M., Roeber, T., Kuegeler, E., Ashcroft, G.: *Turbulence Treatment in Steady and Unsteady Turbomachinery Flows*, Fifth European Conference on Computational Fluid Dynamics ECCOMAS CFD 2010
- [3] Garzon, V.E.: *Probabilistic Aerothermal Design of Compressor Airfoils*, PhD Thesis Dept. of Aeronautics and Astronautics, MIT, 2002
- [4] Garzon, V.E., Darmofal, D.L.: *Impact of Geometric Variability on Axial Compressor Performance*, Journal of Turbomachinery, 125(4):692-703, October 2003
- [5] Hall, K. C., Thomas, J. P., and Clark, W. S.: *Computation of unsteady nonlinear flows in cascades using a harmonic balance technique*, AIAA Journal, 40(5), May, pp. 879–886, 2002

- [6] He, L.: *Efficient approach for analysis of unsteady viscous flows in turbomachines*, AIAA Journal, 36(11), Nov., pp. 2005–2012, 1998
- [7] Lengyel-Kampmann, Bischoff, A., Meyer, R., Nicke, E.: *Design of an Economical Counter-Rotating Fan – Comparison of the Calculated and Measured Steady and Unsteady Results*, ASME Paper GT2012-69587, ASME Turbo Expo Copenhagen, June 2012
- [8] Lengyel, T., Voß, C., Schmidt, T., Nicke, E.: *Design of a counter rotating fan. an aircraft engine technology to reduce noise and CO2 –emissions*, ISABE Paper 2009-1267, 19th ISABE Conference Montreal/Canada, September 2009
- [9] Mileschin, V., Popovyan, A., Korznev, V., Maximov, V., Khaletskiy, Y.: *C-3A aero-acoustic test facility of CIAM & use for VITAL counter rotating fan tests (CRTF application)*. Central Institute of Aviation Motors (CIAM) – Russia; Proceedings of the EU-VITAL –Workshop, 9-10 March 2009, Budapest/Hungary
- [10] Schnell, R., Lengyel-Kampmann, T., Nicke, E.: *Non-deterministic Appraisal of the Impact of geometric Variability on the Aerodynamic Performance of a Blisk-Manufactured Contra-Rotating Turbo Fan*, 21st ISABE Conference, 9.-13. September, Busan/Korea, 2013
- [11] Talbotec, J, Vernet, M.: *Snecma Counter Rotating Fan Aerodynamic Design: Logic&Tests Results*, 27th Intern. Congress of Aeronautical Science ICAS 2010

8 Contact Author Email Address

Rainer Schnell
 German Aerospace Center DLR
 Institute of Propulsion Technology
 Mail to: rainer.schnell@dlr.de

Copyright Statement

The authors confirm that they, and/or their company or organization, hold copyright on all of the original material included in this paper. The authors also confirm that they have obtained permission, from the copyright holder of any third party material included in this paper, to publish it as part of their paper. The authors confirm that they give permission, or have obtained permission from the copyright holder of this paper, for the publication and distribution of this paper as part of the ICAS 2014 proceedings or as individual off-prints from the proceedings.